AIAA JOURNAL
Vol. 34, No. 7, July 1996

Analysis of Compressible Light Dynamic Stall Flow at Transitional Reynolds Numbers

R. D. Van Dyken*
U.S. Naval Air Warfare Center, China Lake, California 93555
and
J. A. Ekaterinaris,† M. S. Chandrasekhara,‡ and M. F. Platzer§
U.S. Naval Postgraduate School, Monterey, California 93943

Numerical and experimental results of steady and light dynamic stall flow over an oscillating NACA 0012 airfoil at a freestream Mach number of 0.3 and Reynolds number of 0.54×10^6 are compared. The experimental observation that dynamic stall is induced from the bursting of a laminar separation bubble points to the role of transition in influencing the flow development. Its modeling, including the changes in transition onset location and transition length with increase in airfoil angle of attack, is critical for computing the dynamic stall flow properly. In this study, the transition onset point is specified suitably and a simple transition length model is incorporated to determine the extent of the laminar separation bubble. The thin-layer approximations of compressible, Reynolds-averaged, Navier–Stokes equations are used for the numerical solution, with an implicit, upwind-biased, third-order-accurate scheme for the numerical integration. Remarkably good agreement with experiments is obtained in steady flow for the pressure and velocity distributions near the leading edge. Oscillatory airfoil flow results compare favorably on the upstroke, but on the downstroke, the computations do not predict the light stall and vorticity shedding that were observed experimentally.

I. Introduction

DYNAMIC stall occurs when an airfoil is pitched rapidly past the static stall angle. Complex flow patterns are produced that present formidable measurement and computational challenges.[1,2] The stall onset behavior changes as the freestream Mach number and Reynolds number are changed. At low Mach numbers and high Reynolds numbers, trailing-edge flow reversal propagates upstream to induce dynamic stall. Even though a separation bubble may form under these conditions, it does not have much influence on unsteady flow separation. However, as the freestream Mach number is increased above 0.2 (Refs. 3 and 4), and compressibility effects take over, dynamic stall becomes leading-edge stall on all airfoils tested until now.[5] At transitional Reynolds numbers, the presence of the laminar separation bubble alters the leading-edge flow character, and thus the stall behavior is affected considerably.

The type of dynamic stall that occurs depends upon the amount by which the static stall angle is exceeded during the pitch-up motion. Deep dynamic stall occurs when the airfoil is pitched to angles significantly above the static stall angle. Light dynamic stall[3] occurs when the static stall angle is exceeded only slightly. The extent, severity, and duration of the separation is significant, yet these are much less than for deep stall. A distinguishing feature of light dynamic stall is that the vertical extent of the viscous zone is of the order of the airfoil thickness, and thus thin-layer Navier–Stokes equations can be used for its analysis.[3]

In the past, many numerical investigations[6–8] of dynamic stall based on laminar flow assumptions have been reported, but they do not adequately model the appropriate dynamic stall flow physics experimentally observed by Carr et al.[4] or Van Dyken and Chandrasekhara[9] and Chandrasekhara and Van Dyken.[10] However, turbulent flow computations have also not been able to reproduce the high-Reynolds-number test results of Carr et al.[4] Analysis of the dynamic stall vortex shedding process for fully turbulent flow conditions was attempted in Refs. 11–16, but these were only partially successful in predicting the details of the flow process. Note that, for purposes of dynamic stall flow control, the prediction of stall onset and associated events is most critical, and to this extent none of the previous computational studies have produced fully satisfactory results.

The complexity of the dynamic stall phenomenon requires a more complete modeling of the underlying flow physics. For this purpose, oscillating airfoil flow studies where incipient stall or light dynamic stall is encountered serve as useful test cases to validate the capability of numerical schemes and turbulence models to predict this complex unsteady flow phenomenon. This paper addresses such a case wherein the flow over a 3-in. chord NACA 0012 airfoil is studied at steady angles of attack and with the airfoil oscillating as $\alpha(t) = 10\,\text{deg} + 2\,\text{deg}\sin\omega t$ at a reduced frequency $k = \pi f c/U_\infty = 0.05$, while experiencing light dynamic stall. The freestream Mach number is 0.3 and the chord-based Reynolds number is 0.54×10^6. The airfoil reaches a maximum angle of attack of 12 deg, which is the same as the static stall angle at $M_\infty = 0.3$, providing the possibility of studying incipient dynamic stall.

The experimental data for comparing and validating the computational results were obtained by mounting the 3-in. chord airfoil between windows in the test section walls of the NASA Ames Compressible Dynamic Stall Facility. The airfoil was oscillated by moving the windows in a sinusoidal motion. The experiments provide a careful nonintrusive documentation of the flow using laser Doppler velocimetry (LDV) and point diffraction interferometry (PDI). The experimental study has clearly established the two-dimensional nature of the flowfield up to the dynamic stall onset angle of attack and even in the attached region of the partially separated flow,[10,17] such as that seen in Fig. 1. The PDI images in Fig. 1 show that a separation bubble forms on the airfoil. This is indicated by the fact that the inner fringes near the leading edge initially run parallel to the upper surface and then turn sharply towards the surface (Figs. 1a and 1b).

Presented as Paper 94-2255 at the AIAA 25th Fluid Dynamics Conferences, Colorado Springs, CO, June 20–23, 1994; received March 1, 1995; revision received March 14, 1996; accepted for publication March 25, 1996.

*Research Scientist, Weapons Division. Member AIAA.
†Research Associate Professor, Navy–NASA Joint Institute of Aeronautics and Department of Aeronautics and Astronautics; currently Senior Research Scientist, Risoe National Laboratory, DK-4000 Roskilde, Denmark. Associate Fellow AIAA.
‡Associate Director and Research Professor, Navy–NASA Joint Institute of Aeronautics and Department of Aeronautics and Astronautics; mailing address M.S. 260-1, NASA Ames Research Center, Moffett Field, CA 94035-1000. Associate Fellow AIAA.
§Director and Professor, Navy–NASA Joint Institute of Aeronautics and Department of Aeronautics and Astronautics. Associate Fellow AIAA.

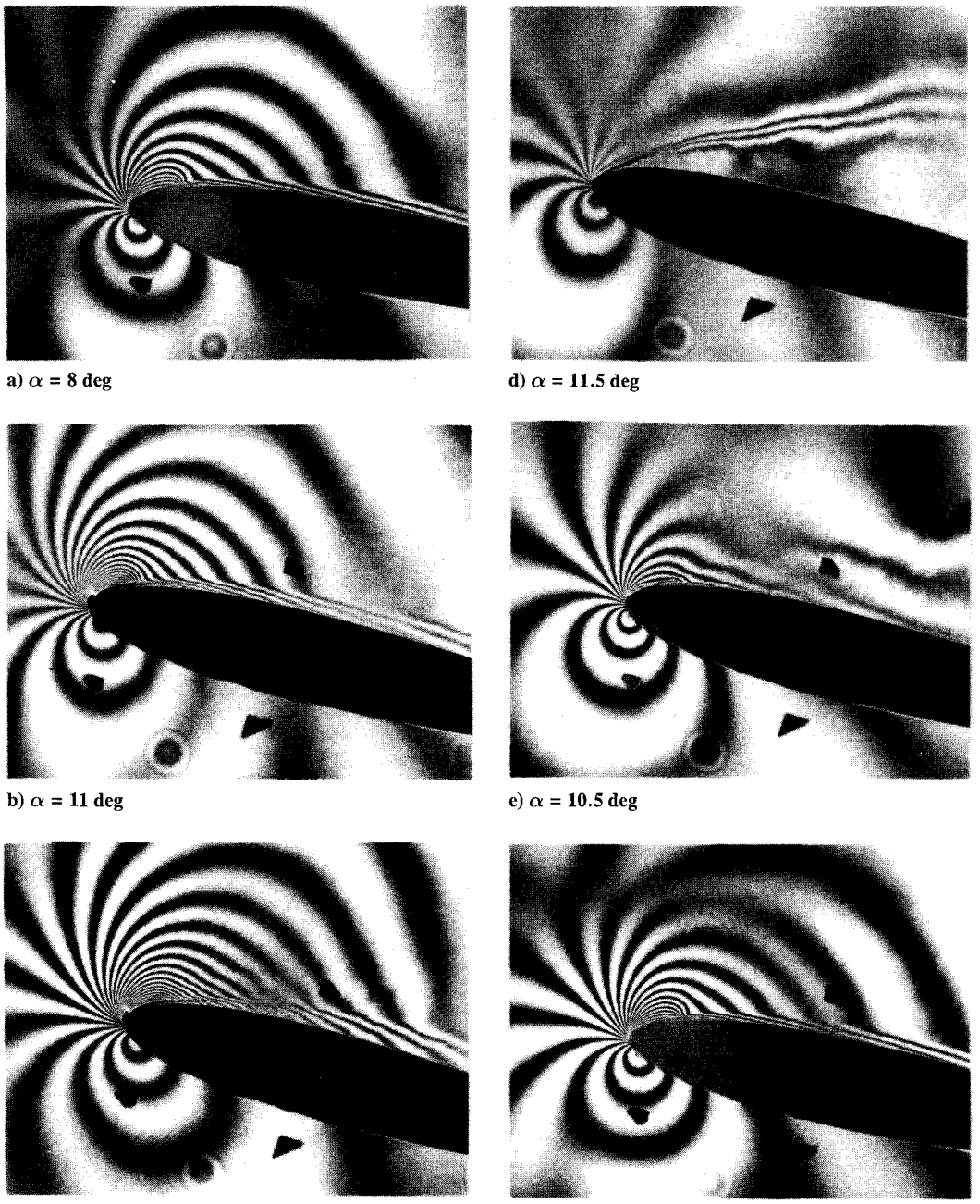

Fig. 1 PDI interferograms of flow over oscillating airfoil; $M_\infty = 0.3$, $\alpha(t) = 10$ deg + 2 deg sin ωt, $k = 0.05$, and $Re_c = 0.54 \times 10^6$.

The outer fringes do not show this trend. At $\alpha = 11.9$ deg (Fig. 1c), additional fringes form on the upper surface, below the bubble, indicating that onset of stall is imminent. As the airfoil pitches down, the dynamic stall vorticity is shed[10] as the flow adapts to the decreasing angle of attack and the rapid changes in pitch rate from positive to negative values. Flow reattachment occurs rapidly from $\alpha = 11.5$ to 10.5 deg (Figs. 1d and 1e), and another bubble forms (Fig. 1f) during reattachment. These PDI images clearly show the formation and development of a separation bubble on the upstroke, its bursting leading to light dynamic stall, the separated shear layer on the downstroke, and flow reattachment later in the cycle. The LDV measurements also support this result.[10] It is thus clear that shear layer transition plays an important role at this Reynolds number, where model-scale data are generally obtained for helicopter applications. It is a challenge for the fluid dynamicist to properly model the physics of the above-described events. In particular, it is critical to model the formation of the separation bubble in compressible flow at transitional Reynolds numbers. To this end, the precise location of transition onset and the extent of transitional flow must be determined as a function of the rapidly changing adverse pressure gradient.

In this paper, computational results are systematically compared with the experimental data set to establish the appropriate transition onset and length parameters to be used in computations. The objective is to closely match the experimental data in hand by incorporating the appropriate fluid flow physics. No effort is made to obtain results for cases where these comparisons cannot be made.

II. Description of the Approach

A. Transition Prediction

Transition prediction methods are based on empirical formulations for boundary-layer flows. These formulations have been used with success for incompressible flows, but the methods bear uncertainties for adverse pressure gradient driven compressible flows. In a recent paper, Ekaterinaris et al.[18] estimated the transition onset

location using the empirical Michel's criterion[19] and the transition length using the Chen–Thyson model.[20] This model is based on data for attached flows and gives the turbulent intermittency γ_{tr} as

$$\gamma_{tr}(x) = 1 - \exp\left[\left(-\frac{u_e^3}{G_{\gamma_{tr}}\nu^2}\right) Re_{x_{tr}}^{-1.34}(x - x_{tr}) \int_{x_{tr}}^{x} \frac{dx}{u_e}\right]$$

Walker et al.[21] also used the Chen–Thyson model in combination with a viscous-inviscid interaction method to compute the separation bubble occurring on a NACA 65-213 airfoil in incompressible flow and $Re_c = 2.4 \times 10^5$. At this low Reynolds number, they found that the transition constant $G_{\gamma_{tr}}$ had to be chosen such that $20 \leq G_{\gamma_{tr}} \leq 40$ to properly compute the separation bubble, as opposed to the required and recommended value of 1200 for high-Reynolds-number flows. Physically, a lower value of the transition constant forces transition to take place over a shorter distance. Recent experiments by Gostelow et al.[22] on the effects of freestream turbulence and adverse pressure gradient on boundary-layer transition show that a change in pressure gradient from zero to even a modest adverse level is accompanied by a severe reduction in transition length.

From the description of the light dynamic stall flow provided, while discussing Fig. 1, it is clear that the flow is dominated by a rapidly changing adverse pressure gradient as the airfoil oscillates. Thus, the transition onset point and length also vary considerably. Given this fact, it is impossible to find or devise a model that satisfactorily represents the transition onset point. Hence, in the present paper, onset of transition is varied systematically from the initial prediction given by Michel's criterion, which is based on high-Reynolds-number data, $Re_c \geq 10^6$. The transition length is varied systematically by varying the $G_{\gamma_{tr}}$ constant in the Chen–Thyson model from an initial estimate given by the Cebeci correlation formula[23]

$$G_{\gamma_{tr}} = \frac{213\left[\log\left(Re_{x_{tr}}\right) - 4.7323\right]}{3}$$

The value that best models the separation bubble behavior observed in experiments of Ref. 10 is used while presenting the results. Some data are presented to show the possible variations in the results if improper values are used. The extreme sensitivity of the flow to these parameters makes it critical to make the choices very carefully. Subsequently, the Baldwin–Barth one-equation model[24] is used for computation of the eddy viscosity in the fully turbulent region.

B. Numerical Implementation

The thin-layer approximation of the compressible, Reynolds-averaged, Navier–Stokes equations for a body-fitted coordinate system (ξ, η) is used for the viscous flow analysis. These equations are as follows:

$$\partial_t \hat{\boldsymbol{q}} + \partial_\xi \hat{\boldsymbol{F}} + \partial_\eta \hat{\boldsymbol{G}} = Re^{-1} \partial_\eta \hat{\boldsymbol{S}}$$

where $\hat{\boldsymbol{q}}$ is the conservative variable vector, $\hat{\boldsymbol{q}} = [\rho, \rho u, \rho v, e]^T$, $\hat{\boldsymbol{F}}$ and $\hat{\boldsymbol{G}}$ are the inviscid flux vectors, and $\hat{\boldsymbol{S}}$ represents the thin-layer approximation of the viscous terms in the normal direction. In the preceding equations, all geometrical dimensions are normalized with the airfoil chord length c; the density ρ is normalized with the freestream density ρ_∞; the Cartesian velocity components (u, v) of the physical domain are normalized with the freestream speed of sound a_∞; and the pressure p is normalized with p_∞.

Details of the numerical techniques are given in Refs. 18 and 24. The inviscid fluxes $\hat{F}$ and $\hat{G}$ are evaluated using Osher's upwinding scheme. For linearization of the left-hand side terms, the flux Jacobian matrices are evaluated by the Steger–Warming flux-vector splitting method. The viscous fluxes $S_{i,k+\frac{1}{2}}$ are computed with central differences.

C. Comparison of Velocity Profiles

The LDV measurements were obtained on a 6×21-point grid in the range $-0.167 \leq x/c \leq 0.167$ and $0.083 \leq y/c \leq 0.167$, in increments of 0.0167 in both directions in an attempt to characterize the separation bubble. The origin of the coordinate system is located at the airfoil leading edge for $\alpha = 0.0$ deg. The computational grid rotates about the point $x/c = 0.25$ and $y/c = 0.0$, whereas the LDV measurement grid remains stationary above the airfoil for the unsteady measurement cases. Data points are interpolated from a 275×81-point computation grid to the experimental grid to get a direct comparison of computed velocities with measured velocities.

D. Uncertainty Analysis

Grid independence was established by comparing the results obtained with a baseline 275×81-point grid and a locally refined 601×161-point grid. In the region around the separation bubble, 16 points were used in the baseline grid and 86 points in the dense grid in the streamwise direction. In the boundary layer, there were 17 and 38 points in the two grids, respectively. A time step of 0.005 was used, and the maximum residuals in steady flow were of the order of 10^{-6} after 4000 time steps. In unsteady flow computations and for a time step of 0.005, the residuals were of the order of 10^{-4}. The slightly larger residual for the unsteady flow is not of any concern since the flow is changing due to the imposed unsteadiness. The unsteady flow solution was started with a converged steady solution for 8-deg angle of attack. The pressure and skin-friction distributions differed by less than 1.5% at a steady angle of attack of 8 deg even at the maximum values of the quantities compared. For example, the suction peaks were -3.40 and -3.45 for the two grids, respectively. Thus, only minor differences were noted in the computed solutions. Unsteady computed solutions were run for three cycles with no differences noted between the second and third cycle. Therefore, results computed during the second cycle are shown in this paper. In what follows, computational results obtained using the 275×81-point grid are presented for both steady and unsteady flows.

The estimated experimental uncertainties are as follows: Mach number of ± 0.005, angle of attack of 0.05 deg, reduced frequency of 0.005, and C_p of $\pm$ 0.2 at $M = 0.3$.

The uncertainty in C_p depends on the fringe number under consideration and is estimated to be one fringe (± 0.2) for the flow in general. Near the suction peak, however, it is estimated that three fringes were undetected, leading to a larger uncertainty of about -0.6. Uncertainty in the LDV data is estimated to be 5% in attached flow.

III. Results and Discussion

A. Steady-State Flow Studies

As pointed out by Walker et al.,[21] the computation of low-Reynolds-number flows over airfoils with separation bubbles depends critically on the transition onset location and transition length. The validity of Michel's criterion for determination of transition onset at a Reynolds number of 0.54×10^6 is yet to be fully verified. Straightforward use of Michel's criterion for the present flow predicted a transition onset range of $0.025 \geq x/c \geq 0.009$ for steady flow in the angle-of-attack range $6 \leq \alpha \leq 12$ deg. This range of transition onset locations predicted separation bubbles that were much smaller than the experimentally determined ones using PDI, and the pressure peaks were far in excess of PDI deduced values. Transition onset locations farther aft on the airfoil surface are expected for lower-Reynolds-number flows. For this reason, the transition onset location was varied in the present study, and its effects on the computed pressure and skin-friction distribution were investigated systematically. Figure 2a shows that the computed separation bubble length along the airfoil surface as determined by the extent of the negative skin-friction region on the plots increased by 150% when transition onset was moved aft by a mere 1% of chord from $x/c = 0.03$ to 0.04. If the transition onset location was specified too far aft from the leading edge on the airfoil surface, the overall numerical scheme became unstable because of the development of a very large, nonphysical reverse flow region and formation of vortical structures at the airfoil leading edge.

A similar effect occurred when the transition length was changed by controlling the $G_{\gamma_{tr}}$ constant. Increasing $G_{\gamma_{tr}}$ yielded increased transition length and longer separation bubbles. Application of Cebeci's correlation formula[23] resulted in a transition constant range of $380 \leq G_{\gamma_{tr}} \leq 460$ for steady angles of incidence from 6–12 deg. As can be seen from the skin-friction distribution in Fig. 2b, an order of magnitude change in $G_{\gamma_{tr}}$, from 50 to 460, nearly doubled the bubble length along the airfoil surface. Use of a $G_{\gamma_{tr}}$ constant of 50

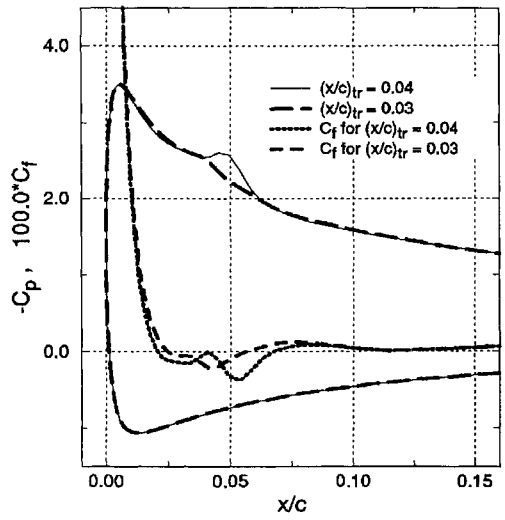

Fig. 2a Effect of transition onset location on steady flow pressure and skin-friction distributions; $M_\infty = 0.3$, $\alpha = 8.0$ deg, $Re_c = 0.54 \times 10^6$, and $G_{\gamma_{tr}} = 200$.

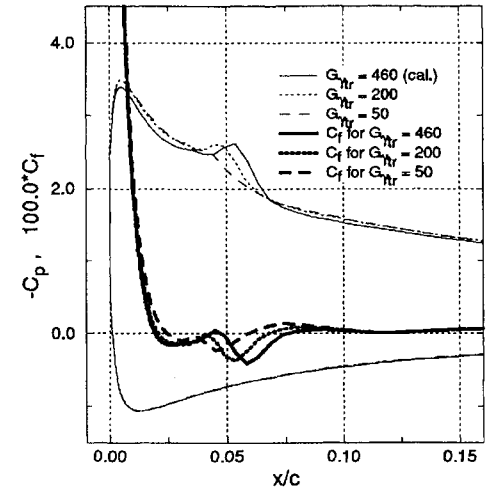

Fig. 2b Effect of transition constant $G_{\gamma_{tr}}$ on steady flow pressure and skin-friction distributions; $M_\infty = 0.3$, $\alpha = 8.0$ deg, $Re_c = 0.54 \times 10^6$, and $(x/c)_{tr} = 0.04$.

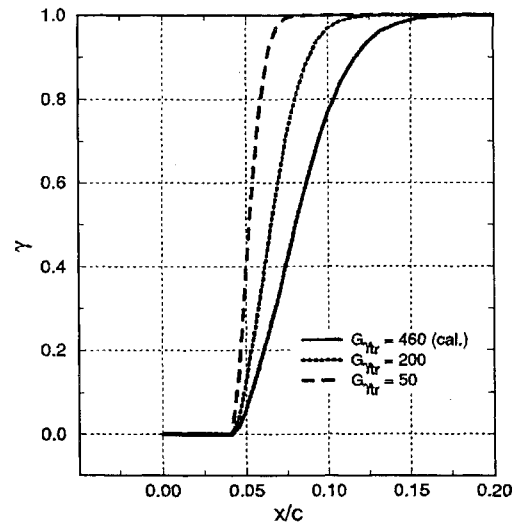

Fig. 2c Effect of transition constant $G_{\gamma_{tr}}$ on intermittency distribution; $M_\infty = 0.3$, $\alpha = 8.0$ deg, $Re_c = 0.54 \times 10^6$, and $(x/c)_{tr} = 0.04$.

resulted in separation bubbles that were much smaller than experimentally measured. A value of 460 for $G_{\gamma_{tr}}$ obtained from the formula for $\alpha = 8$ deg, when used together with the more aft transition onset locations, yielded earlier flow reattachment and a smaller secondary separation bubble. Thus, a combination of transition onset locations aft of those predicted by Michel's criterion and a $G_{\gamma_{tr}}$ constant value of 200 were chosen for the bulk of the computations because the resultant numerical solutions most closely matched the experimental results for the test case of 8-deg angle of incidence.

The effect of $G_{\gamma_{tr}}$ variation in altering the transition length is shown in Fig. 2c. The intermittency distribution plotted in it shows a very gradual transition extending between $x/c = 0.04$ to 0.15 for a value of 460, which decreases rapidly to x/c between 0.04 to 0.06 for a value of 50. For a value of 200, an intermediate transition length is observed. This clearly establishes the need to control the parameter to obtain good comparison with separation bubble length as the angle of attack is increased.

Figure 3a shows the comparison between the PDI deduced and the computed pressure coefficient distributions at $\alpha = 6$ deg in steady flow with transition onset at $(x/c)_{tr} = 0.04$. For this angle of attack, no separation bubble was found in the experiment. Also, the computed skin friction remains positive and hence does not indicate a separation bubble. The pressure distributions agree very well with each other. Any differences seen are within the experimental and computational uncertainties.

In Fig. 3b, a similar plot is shown for $\alpha = 8$ deg in steady flow for $(x/c)_{tr} = 0.034$. As can be expected, the transition onset location moves towards the leading edge as the angle of attack is increased. Agreement between the two sets of data is good. However, around the bubble, small differences appear. The measured suction peak is slightly lower than the computed value, but it is still within the uncertainty band. The location of first flow separation ($C_f = 0$ value at $x/c \approx 0.025$ where the flow is still laminar) agrees closely with the start of the plateau in the measured pressure distribution. Since $C_f = 0$ is a reliable indicator of flow separation, this agreement allows one to determine the beginning of the bubble by the beginning of the plateau in the pressure distribution. It is well known that the end of the separation bubble cannot be precisely determined from the pressure distributions alone.[25,26] In general, it is near the pressure recovery region. The reappearance of a positive value of C_f in the vicinity of the pressure recovery region of the measured pressure distribution confirms agreement between the two sets of data.

Similar results can be seen in Fig. 3c for $\alpha = 10$ deg for which the transition onset point moves further upstream to $(x/c)_{tr} = 0.0225$. The beginning of the bubble agrees to within one fringe in the pressure plot when compared with the skin-friction distribution. The total bubble length also agrees well. The somewhat larger differences between the computed and measured pressure distributions can be attributed to the slightly positive skin-friction value at $x/c \approx 0.025$, suggesting a secondary bubble formation is predicted by the numerical solution. Hence, the computed $(-C_p)$ pressure distributions show a second rise and a subsequent fall. The measured suction peak appears at a slightly larger x/c location as a result of the downstream displacement of the light beam caused by optical distortions introduced by the large local density changes present in the flow at high angles of attack.[27]

Figure 4 shows a comparison of computed and measured (PDI) density contours at the leading edge of the airfoil at $\alpha = 10$ deg. Twenty-seven density contour levels are shown with a $\Delta\rho/\rho_0 = 0.0085$ per dark fringe, resulting in a predicted peak Mach number of 0.72 over the upper surface of the airfoil. In this figure, the separation bubble is represented by the contours that run parallel to the airfoil surface before turning sharply towards the airfoil surface, as explained while discussing Fig. 1. The vertical extent of the separation bubble as determined by the fringe lines that run parallel to the surface is greater than that for the predicted separation bubble. The reasons given for the differences observed in Fig. 3 also account for the slightly longer separation bubble and its origin slightly further upstream of the measured location. Overall, the agreement seen is very good considering the fact that PDI gives an instantaneous documentation of the flow and the differences seen (in this overly magnified figure) are generally less than the one fringe uncertainty of the technique.

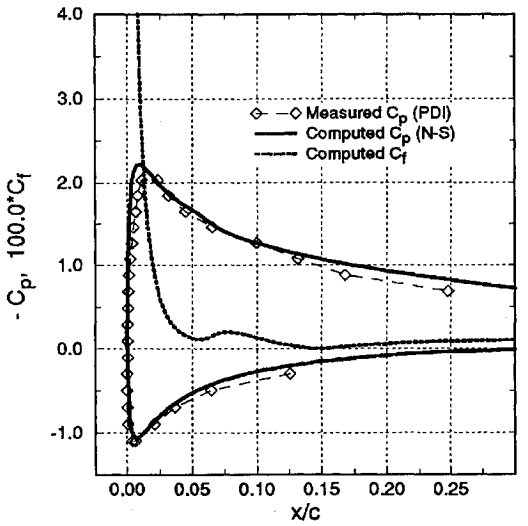

a) α = 6.0 deg and $(x/c)_{tr}$ = 0.04

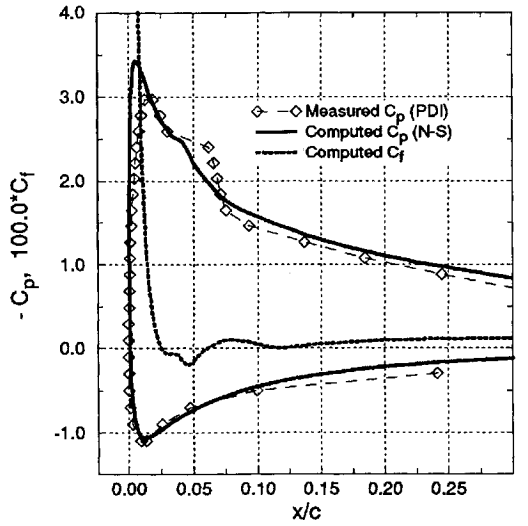

b) α = 8.0 deg and $(x/c)_{tr}$ = 0.034

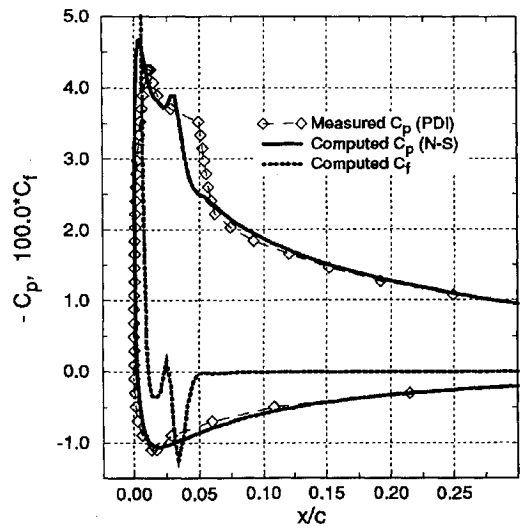

c) α = 10.0 deg and $(x/c)_{tr}$ = 0.0225

Fig. 3 Comparison of computed and measured pressure distributions and computed skin friction in steady flow, M_∞ = 0.3 and Re_c = 0.54 × 10^6.

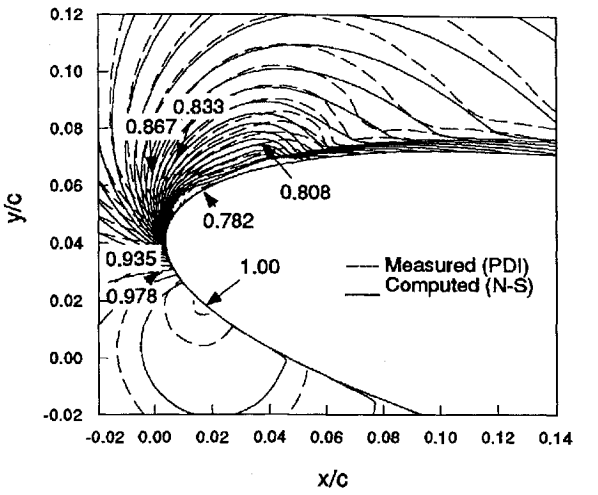

Fig. 4 Computed and measured density contours near airfoil leading edge in steady flow; M_∞ = 0.3, α = 10.0 deg, and Re_c = 0.54 × 10^6.

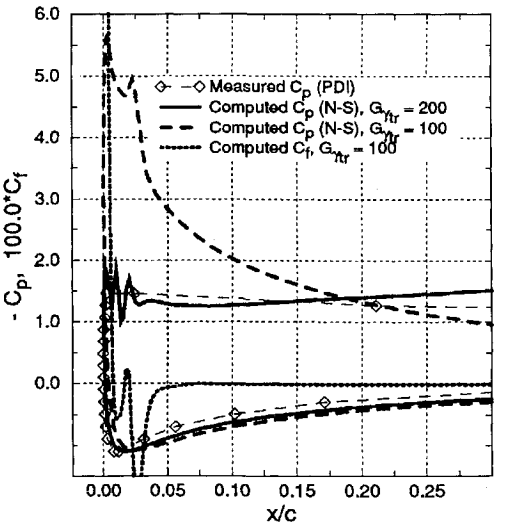

Fig. 5 Comparison of computed and measured pressure distributions and computed skin friction near static stall angle; M_∞ = 0.3, α = 12.0 deg, and Re_c = 0.54 × 10^6.

Figure 5 presents an interesting comparison of the different computed pressures with the PDI experiment at $\alpha = 12$ deg. Note that the experiments showed borderline flow separation at $\alpha = 12$ deg for $M_\infty = 0.3$. The flow was thus intermittently attached at which instant a large suction peak was produced. This could be attributed to the unsteady nature of flow separation at stall onset. For the case of transition onset at $x/c = 0.017$ and $G_{\gamma_{tr}} = 200$, the computations reproduced the experimental results well by predicting stall correctly. Small changes in the transition onset location and $G_{\gamma_{tr}}$ values yielded a completely attached flow with high levels of suction. Thus, it appears that the numerical modeling adequately represents the physical flow in the wind tunnel for steady angles of attack.

B. Unsteady Flow Studies

Figure 6 gives pressure distributions from the PDI measurements for the unsteady flow case. Figure 6a gives surface pressure coefficients for the upstroke from $\alpha = 8$ to 11 deg, and Fig. 6b gives surface pressure coefficients for the downstroke from $\alpha = 12$ to 9 deg. It is clear from Fig. 6a that a separation bubble exists on the airfoil throughout the upstroke (also see Fig. 1). The peak suction pressure increases with angle of attack as expected. However, as the top of the oscillation cycle is approached at $\alpha = 12$ deg, the pitch rate decreases to zero and the suction level drops from $C_p = -4.3$ at $\alpha = 11$ deg to -3.8 at 12 deg. During the downstroke, light dynamic stall occurs through the shedding of the vorticity at $\alpha = 11.5$ deg with the flow still separated at $\alpha = 11$ deg. As a consequence, the peak

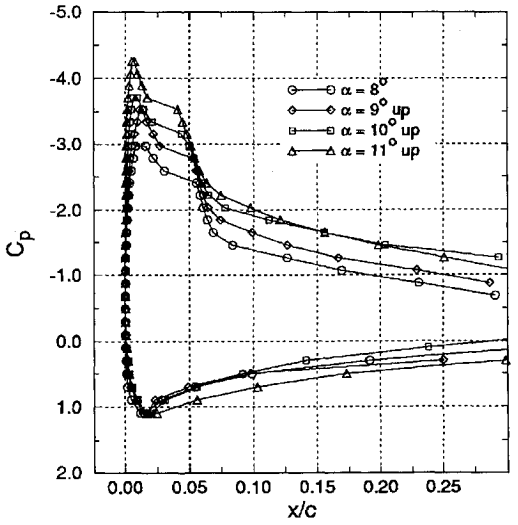

a) Upstroke

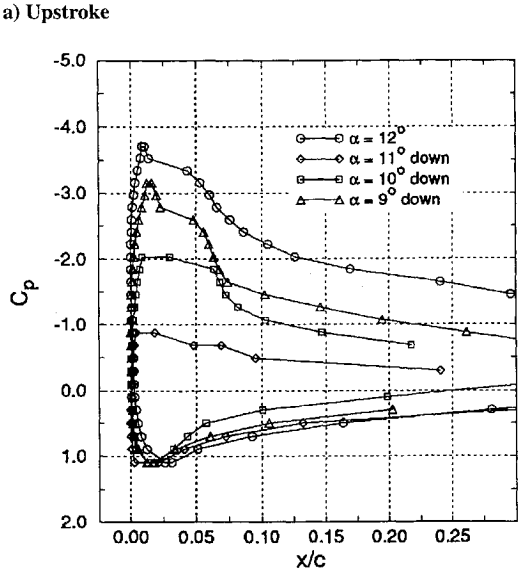

b) Downstroke

Fig. 6 Measured surface pressure distributions; $M_\infty = 0.3$, $\alpha(t) = 10$ deg + 2 deg sin ωt, $k = 0.05$, and $Re_c = 0.54 \times 10^6$.

suction pressure drops significantly to $C_p = -0.9$. As flow reattachment progresses, increasing suction pressures develop again. Eventually, at $\alpha = 9$ deg, a flow pattern similar to the upstroke is reestablished. However, a comparison of Figs. 6a and 6b for $\alpha = 9$ deg on the up- and downstrokes shows that pressures during the downstroke are slightly lower.

Transition onset locations and transition length constants predicted by Michel's criterion and Cebeci's formula for the unsteady case were very similar to the steady flow cases. The ranges were $0.012 \leq x/c \leq 0.02$ and $370 \leq G_{Re} \leq 410$, respectively. As was done for the steady flow case, these parameters were adjusted during the oscillatory cycle to give the best comparison with PDI results. A comparison of computed and measured (PDI) density contours around the leading edge of the airfoil at $\alpha = 10$ deg on the upstroke in the oscillatory cycle are shown in Fig. 7. The range and increment of computed density values for the contours were set identical to the PDI data set. Twenty-four contours are plotted, with the last one corresponding to a peak Mach number of 0.67 over the upper surface of the airfoil. The numerical predictions for the oscillatory airfoil flow case show about the same level of agreement observed for the steady-state results, for the same reasons described earlier.

The measured and computed velocity profiles are compared in Fig. 8 at selected streamwise stations. These profiles have been normalized by the velocity at the edge of the computational grid U_e ($y/c = 0.167$), for each x/c station. Figure 9a shows very good agreement between the two sets of data at $x/c = -0.033$ upstream

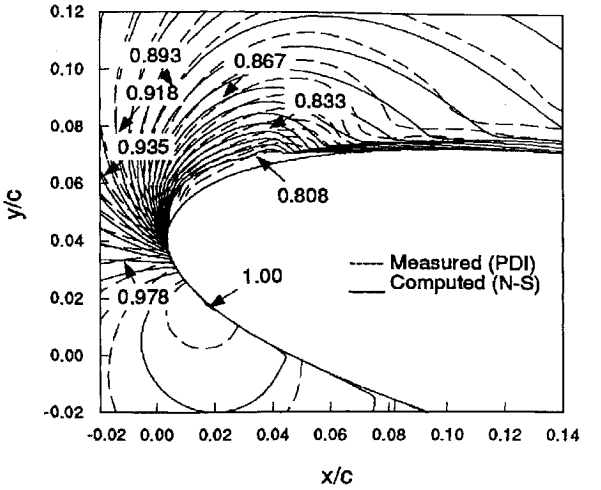

Fig. 7 Computed and measured density contours over oscillating airfoil near leading edge; $M_\infty = 0.3$, $\alpha(t) = 10$ deg + 2 deg sin $\omega t = 10.0$ deg upstroke, $k = 0.05$, and $Re_c = 0.54 \times 10^6$.

of the airfoil. Likewise, all velocity profile comparisons at x/c locations forward of $x/c = -0.033$ were found to be in excellent agreement. Although the computed distributions are shown down to the surface, the measured values end at slightly higher y/c values since points closer to the airfoil surface could not be optically accessed because of laser beam blockage by the airfoil. At $x/c = 0.0$, i.e., near the airfoil leading edge at this angle of attack, the agreement is excellent for higher y/c locations, but differences of about 3% are seen closer to the airfoil surface. It should be noted that these differences are within the accuracy of the laser velocimetry system. Figures 8b and 8c both show the same trend observed for the outer grid points at $x/c = 0.033$. However, a large difference of about 30% is seen at $y/c = 0.083$. The vertical extent of the measured separation bubble above the airfoil surface at this location was determined to be about 2% chord in Ref. 10. From the steady-state comparisons, it is seen that the computations generally predicted a separation bubble that was smaller in the vertical direction. Hence, differences between computed and measured velocities are attributed to a larger separation bubble that was observed in the experiments. It is further possible that particle lag effects may have influenced the measurements because of the rapid flow acceleration around the leading edge and the subsequent sudden deceleration that produces the separation bubble over the airfoil. Similar features can be seen in Fig. 8d at $x/c = 0.067$. As the flow reattaches and proceeds normally over the airfoil, as shown in Figs. 8e and 8f, once again the agreement between the two data sets improves to within experimental uncertainties. Thus, it can be said that inclusion of the transition phenomenon has resulted in a more accurate computation of the flow at the Reynolds number for which the comparison is made.

Figure 9a compares measured and computed pressure distributions at the extremes of the oscillation cycle, $\alpha = 8$ and 12 deg. There is reasonable agreement between the predicted and measured pressure distributions at $\alpha = 8$ deg. The computed skin-friction distribution indicated a separation bubble comparable to the measured one. At $\alpha = 12$ deg, on the other hand, the computed suction pressures significantly overshoot the measured ones, but the computed skin friction still indicates a bubble comparable to the measured one. As expected, the onset of stall is delayed during the upstroke.

Figure 9b shows the computed and measured pressure distributions for $\alpha = 10$ deg, during both the upstroke and the downstroke. The computed skin-friction distributions are also shown. It is apparent from this comparison that the computations fail to capture the shedding of the dynamic stall vortex during the airfoil downstroke, which was found in the experiments. This aspect of the problem requires further study. Therefore, it is not discussed any more in the present paper. The comparison between measured and computed pressure distributions during the upstroke is not as good as in the steady flow case (Fig. 3c), but this is expected because the computations do not predict light stall during the downstroke.

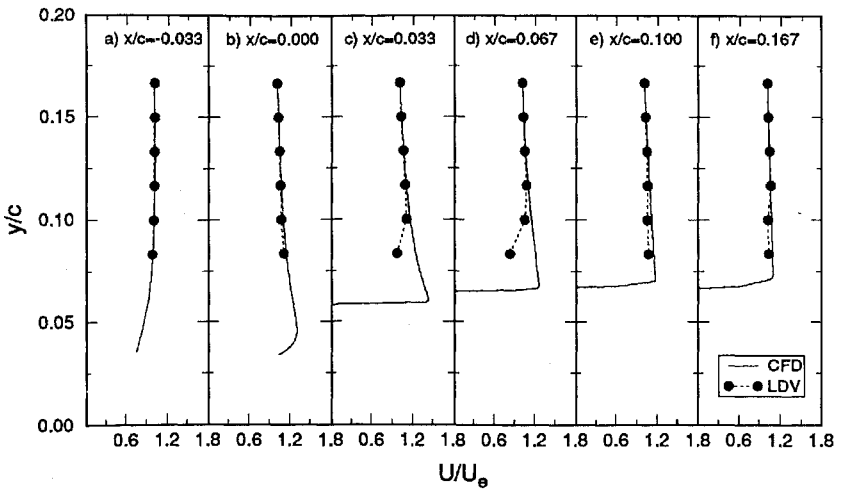

Fig. 8 Computed and measured velocity profiles (U/U_e) over airfoil; $M_\infty = 0.3$, $\alpha(t) = 10$ deg + 2 deg sin $\omega t = 8.0$ deg, $k = 0.05$, and $Re_c = 0.54 \times 10^6$.

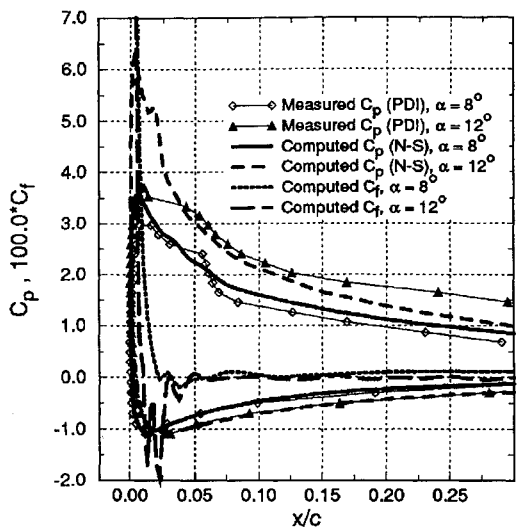

a) α = 8.0 and 12.0 deg

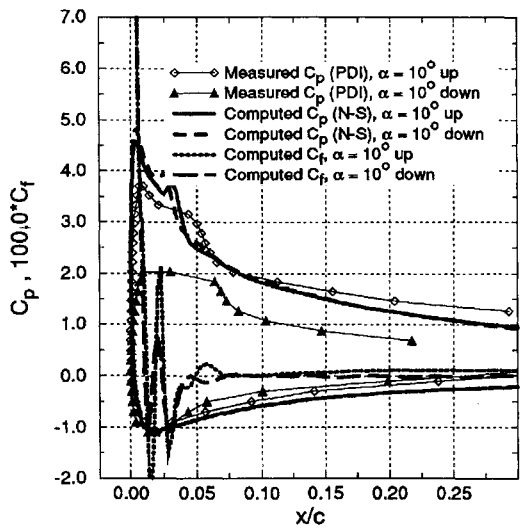

b) α = 10.0 deg up and 10.0 deg down

Fig. 9 Comparison of computed and measured pressure distributions and computed skin friction over oscillating airfoil; $M_\infty = 0.3$, $\alpha(t) = 10$ deg + 2 deg sin ωt, $k = 0.05$, and $Re_c = 0.54 \times 10^6$.

IV. Conclusions

The experimental observation that light dynamic stall is influenced by the formation of a laminar separation bubble at low Reynolds number points to the need of including details of the transition phenomenon over the airfoil to properly compute the flow. Based on this knowledge, the thin-layer approximation of the compressible, Reynolds-averaged Navier–Stokes equations were applied to compute the unsteady flow over an oscillating NACA 0012 airfoil at a Reynolds number of 0.54×10^6. The study revealed that it is absolutely necessary to account for the movement of the transition onset point and changes in the transition length as the airfoil angle of attack changes to obtain good agreement with experimental results, especially in regards to predicting the laminar separation bubble that dominates the flowfield. Because it was found that the length of the bubble critically depended on the transition constant value in the Chen–Thyson model, a systematic analysis revealed a value of 200 as appropriate for the flow under consideration. This value is considerably different from the value of 1200 used for high-Reynolds-number flows. A better transition model is required to obtain a more accurate representation of the flow physics during airfoil oscillatory motion. This most likely requires use of stability theory. Nevertheless, agreement between computations and experiments for steady-state cases was satisfactory.

Acknowledgments

The investigation was supported by the U.S. Naval Air Warfare Center, Weapons Division, China Lake, CA, monitored by C. Porter and D. Siegel, and by the U.S. Army Research Office, Durham, NC, ARO-MIPR-125-93, monitored by T. L. Doligalski.

References

[1]McCroskey, W. J., "Unsteady Airfoils," *Annual Review of Fluid Mechanics*, Vol. 14, 1982, pp. 285–311.

[2]Carr, L. W., "Progress in Analysis and Prediction of Dynamic Stall," *Journal of Aircraft*, Vol. 25, No. 1, 1988, pp. 6–17.

[3]McCroskey, W. J., "The Phenomenon of Dynamic Stall," NASA TM-81264, March 1981.

[4]Carr, L. W., McAlister, K. W., and McCroskey, W. J., "Analysis of the Development of Dynamic Stall Based on Oscillating Airfoil Experiments," NASA TN D-8382, Jan. 1977.

[5]Carr, L. W., and Chandrasekhara, M. S., "An Assessment of the Impact of Compressibility on Dynamic Stall," AIAA Paper 95-0779, Jan. 1995.

[6]Visbal, M. R., and Shang, J. S., "Investigation of the Structure Around a Rapidly Pitching Airfoil," *AIAA Journal*, Vol. 27, No. 8, 1989, pp. 1044–1055.

[7]Ghia, K. N., Yang, Y., Oswald, G. A., and Ghia, U., "Study of the Role of Unsteady Separation in the Formation of Dynamic Stall Vortex," AIAA Paper 92-0196, Jan. 1992.

[8]Knight, D. D., and Choudhuri, P. G., "Two Dimensional Unsteady Leading-Edge Separation on a Pitching Airfoil," AIAA Paper 93-2977, July 1993.

[9]Van Dyken, R. D., and Chandrasekhara, M. S., "Leading Edge Velocity Field of an Oscillating Airfoil in Compressible Dynamic Stall," AIAA Paper 92-0193, Jan. 1992.

[10]Chandrasekhara, M. S., and Van Dyken, R. D., "LDV Measurements in Dynamically Separated Flows," *Proceedings of the Fifth Laser Anemometry Conference, Advances and Applications*, Vol. 2052, Society of Photo-Optical Instrumentation Engineers, Bellingham, WA, 1993, pp. 305–312.

[11]Wu, J. C., Huff, D. L., and Sankar, L. N., "Evaluation of Three Turbulence Models in Static Air Loads and Dynamic Stall Predictions," *Journal of Aircraft*, Vol. 27, No. 4, 1990, pp. 382–384.

[12]Dindar, M., and Kaynak, U., "Effect of Turbulence Modeling on Dynamic Stall of a NACA-0012 Airfoil," AIAA Paper 92-0027, Jan. 1992.

[13]Rizetta, D. P., and Visbal, M. R., "Comparative Numerical Study of Two Turbulence Models for Airfoil Static and Dynamic Stall," *AIAA Journal*, Vol. 31, No. 4, 1993, pp. 784–786.

[14]Srinivasan, G. R., Ekaterinaris, J. A., and McCroskey, W. J., "Dynamic Stall of an Oscillating Wing, Part 1: Evaluation of Turbulence Models," AIAA Paper 93-3403, Aug. 1993.

[15]Grohsmeyer, S. P., Ekaterinaris, J. A., and Platzer, M. F., "Numerical Investigation of Leading Edge Geometries on Dynamic Stall of Airfoils," AIAA Paper 91-1798, June 1991.

[16]Ekaterinaris, J. A., "Compressible Studies on Dynamic Stall," AIAA Paper 89-0024, Jan. 1989.

[17]Ahmed, S., and Chandrasekhara, M. S., "Reattachment Studies of an Oscillating Airfoil Dynamic Stall Flowfield," *AIAA Journal*, Vol. 31, No. 4, 1994, pp. 1006–1012.

[18]Ekaterinaris, J. A., Chandrasekhara, M. S., and Platzer, M. F., "Analysis of Low Reynolds Number Airfoil Flows," *Journal of Aircraft*, Vol. 32, No. 3, 1995, pp. 625–630.

[19]Cebeci, T., and Bradshaw, P., "Analysis of Turbulent Shear Layers," *Momentum Transfer in Boundary Layers*, Hemisphere, Washington, DC, 1977, pp. 153–212.

[20]Chen, K. K., and Thyson, N. A., "Extension of Emmons Spot Theory to Flows on Blunt Bodies," *AIAA Journal*, Vol. 9, No. 5, 1971, pp. 821–825.

[21]Walker, G. J., Subroto, P. H., and Platzer, M. F., "Transition Modeling Effects on Viscous/Inviscid Interaction Analysis of Low Reynolds Number Airfoil Flows Involving Laminar Separation Bubbles," ASME Paper 88-GT-32, American Society of Mechanical Engineers, New York, June 1988.

[22]Gostelow, J. P., Blunden, A. R., and Walker, G. J., "Effects of Free-Stream Turbulence and Adverse Pressure Gradients on Boundary Layer Transition," ASME Paper 92-GT-380, American Society of Mechanical Engineers, New York, June 1992.

[23]Cebeci, T., "Essential Ingredients of a Method for Low Reynolds Number Airfoils," *AIAA Journal*, Vol. 27, No. 12, 1989, pp. 1680–1688.

[24]Ekaterinaris, J. A., and Menter, F. R., "Computation of Oscillating Airfoil Flows with One- and Two-Equation Turbulence Models," *AIAA Journal*, Vol. 32, No. 12, 1994, pp. 2359–2365.

[25]Gaster, M., "The Structure and Behavior of Separation Bubbles," Aeronautical Research Council, ARC R&M 3595, London, March 1967.

[26]Tani, I., "Low Speed Flows Involving Bubble Separations," *Progress in Aeronautical Sciences*, Vol. 5, 1964, pp. 70–103.

[27]Cho, Y. C., Carr, L. W., and Chandrasekhara, M. S., "Corrections to Fringe Distortions due to Flow Density Gradients in Optical Interferometry," AIAA Paper 93-0631, Jan. 1993.